Computer Methods in Biomechanics and Biomedical Engineering
Vol. 11, No. 3, June 2008, 235–242

Taylor & Francis
Taylor & Francis Group

TECHNICAL NOTE

Dynamic accuracy of inertial measurement units during simple pendulum motion

M.A. Brodie*, A. Walmsley and W. Page

Massey University, Wellington, New Zealand

(*Received 1 November 2006; final version received 14 March 2008*)

A motion measurement system based on inertial measurement units (IMUs) has been suggested as an alternative to contemporary video motion capture. This paper reports an investigation into the accuracy of IMUs in estimating 3D orientation during simple pendulum motion. The IMU vendor's (XSens Technologies) accuracy claim of 3° root mean squared (RMS) error is tested. IMUs are integrated electronic devices that contain accelerometers, magnetometers and gyroscopes. The motion of a pendulum swing was measured using both IMUs and video motion capture as a reference. The IMU raw data were processed by the Kalman filter algorithm supplied by the vendor and a custom fusion algorithm developed by the authors. The IMU measurement of pendulum motion using the vendor's Kalman filter algorithm did not compare well with the video motion capture with a RMS error of between 8.5° and 11.7° depending on the length and type of pendulum swing. The maximum orientation error was greater than 30°, occurring approximately eight seconds into the motion. The custom fusion algorithm estimation of orientation compared well with the video motion capture with a RMS error of between 0.8° and 1.3°. Future research should concentrate on developing a general purpose fusion algorithm and vendors of IMUs should provide details about the errors to be expected in different measurement situations, not just those in a 'best case' scenario.

Keywords: inertial measurement units; accelerometer; calibration; motion capture; dynamic accuracy; sensor fusion

Introduction

Inertial measurement units (IMUs) are integrated electronic devices that contain accelerometers, magnetometers and gyroscopes. The purpose of this paper is to investigate and improve on the accuracy of IMU measurement of dynamic orientation. A simple pendulum was used because the motion is repeatable and predictable. It is similar to some limb motions in human ambulation and has few motion artefacts to complicate the measurement. If a pendulum swing can be measured accurately with an IMU, then motion capture systems based on IMUs for use in biomechanical research might be considered feasible.

IMUs produce raw data in a local reference frame. Typically a Kalman type filter (XSens Technologies B.V. 2004; Luinge and Veltink 2005; Pfau et al. 2005; Giansanti et al. 2007; Luinge et al. 2007; Supej 2007; Waegli et al. 2007) is used to process the raw data to obtain orientation and measurements in the global reference frame. To capture human motion, segmental movement is measured by an IMU attached to each of the body segments and relative segment positions are obtained by attaching a distal segment to the known position of a proximal joint centre. To obtain gross global movement additional constraints are required, such as data from a Global Positioning System (GPS) receiver.

All the IMUs used in the experiments reported here were MT9 sensors from XSens Technologies. Technical information about the IMU used in this experiment is available in a companion paper, Brodie et al. (2007). No details were provided by XSens about the internal workings of the Kalman filter supplied with the IMUs except that dynamic orientation accuracy is 'less than 3° RMS (XSens Technologies B.V. 2004)'. This is consistent with the findings of Luinge and Veltink (2005):

> Although the problem of integration drift around the global vertical continuously increased in the order of $0.5°s^{-1}$, the inclination estimate was accurate within 3° RMS.

The vendor's specification also comes with the following fine print 'may depend on the type of motion measured', which leads the authors to believe more research is required to determine what 'type of motion' is able to be measured accurately. It is presumed that the Kalman filter implementation is similar to that used by Luinge and Veltink (2005) with the addition that the magnetometer data are used to prevent heading drift (integration drift around the global vertical).

The variability in accuracy of the orientation data obtained from IMUs is reflected in the variability of results in published literature. Giansanti et al. (2007) used IMUs

*Corresponding author. Email: m.a.brodie@massey.ac.nz

ISSN 1025-5842 print/ISSN 1476-8259 online

DOI: 10.1080/10255840802125526
http://www.informaworld.com

to measure trunk orientation in the sit-to-stand task. The authors reported a maximum orientation error of 0.5° in trunk pitch using a fusion algorithm specially designed for the single task. Luinge and Veltink (2005) also measured trunk orientation in a box stacking task. The RMS orientation error was $<3°$ for movement speeds of up to one box stacked every 2 seconds. The orientation error increased as the lifting rate increased. But the maximum movement speed tested was much slower than that of distal limb segments in many human movements.

In contrast, Pfau et al. (2005) used IMUs to measure the dynamic orientation of a horse's trunk during cantering. In this paper the orientation error was reported as a median error, 5.4° about the roll axis. Since the errors were probably not normally distributed about the mean, the maximum error was probably considerably larger than 5.4°. In a recent paper, Luinge et al. (2007) compared IMU estimates of arm orientation during everyday tasks to orientation estimates obtained from video motion capture. Orientation differences accumulated at rates up to $0.6° s^{-1}$ leading to orientation differences of up to 80° over the duration of the tasks. To reduce the orientation differences constraints were applied on the abduction angle of the elbow, which reduced the maximum orientation differences to 40°. The authors concluded that either poor sensor to segment calibration or heading drift were the source of the error, but apparently did not consider that IMU error might also be related to the nature of each task. For the tasks tested the error accumulated fastest during teeth brushing, which was the longest task. It is probable that teeth brushing was also the most dynamic task in terms of the frequency and rapidity of direction changes and this caused the error to accumulate quickly.

In a sport context (skiing) Waegli et al. (2007); Supej (2007) and Brodie et al. (2005, 2007, 2008) have made measurements using IMUs. Supej did not assess the accuracy of the IMUs used. Waegli reported measurement of ski orientation using a custom Kalman filter algorithm with a standard deviation of $<2°$. There appear to be two issues with Waegli's paper. First, ski orientation was reported but it seems the IMU was attached to the athlete's shank, which was then mathematically coupled to a GPS receiver attached to the athlete's ski. Second, no reference system was used to determine the orientation error of the ski. The error reported is in agreement with Brodie et al. (2008) who estimated a maximum error of 5° for ski orientation and other reports of 3° RMS error, (XSens Technologies B.V. 2004; Luinge and Veltink 2005) but contradicts reports made in other dynamic situations. (Pfau et al. 2005; Luinge et al. 2007)

Alternatives to Kalman filters, such as particle filters, could be used to obtain orientation measurements from IMUs in real time. Since 2005, Brodie et al. (2005) have suggested the use of fusion algorithms for iterative post processing of IMU data. Examples of motion capture using IMUs and fusion algorithms are available in the electronic version of a recent publication (Brodie et al. 2008). Further information on the development of fusion algorithms to obtain centre of mass trajectory is also available (Brodie et al. 2007).

Data processing

Fusion algorithm overview

The MATLAB code for the simple bidirectional fusion algorithm in this paper is available from the authors. The algorithm fused a static estimate of orientation (from the accelerometers and magnetometers) with a continuous integral estimate of orientation (from the gyroscopes). As the data were not required in real time the fusion algorithm presented here used the complete data to estimate the orientation of the IMU at each point in time. A simple block diagram of a fusion algorithm is shown in Figure 1.

An example of the fusion process for a data set is shown in Figure 2. The static estimate of orientation, dark blue dots, is only accurate when the pendulum is stationary ($5\,s > t > 30\,s$). The static estimate is only normally distributed about the true orientation, when motion is quasi static ($7\,s < t < 8.5\,s$). The continuous estimate based on the integration of the gyroscope data, light red line, contains integration drift. This low frequency drift is a result of gyroscope bias and noise. The fused estimate, black line, is obtained by correcting the low frequency drift of the gyroscope estimate with information from the static estimate.

The static orientation estimate

An orientation measurement requires the rotation in each of three rotational degrees of freedom to be specified. The accelerometers provide information about pitch and roll while the magnetometers provide information about heading. A more detailed explanation of the calculation is given by Brodie et al. (2007). The orientation matrix ($\mathbf{R}_{Global}$) that describes the sensor orientation in the global reference frame may be obtained from the local axes (Equation (1)). The local axes are derived from the IMU's accelerometers and magnetometers, which measure the

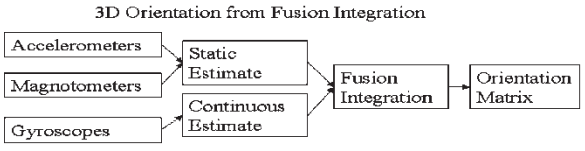

Figure 1. A general outline of the fusion integration process.

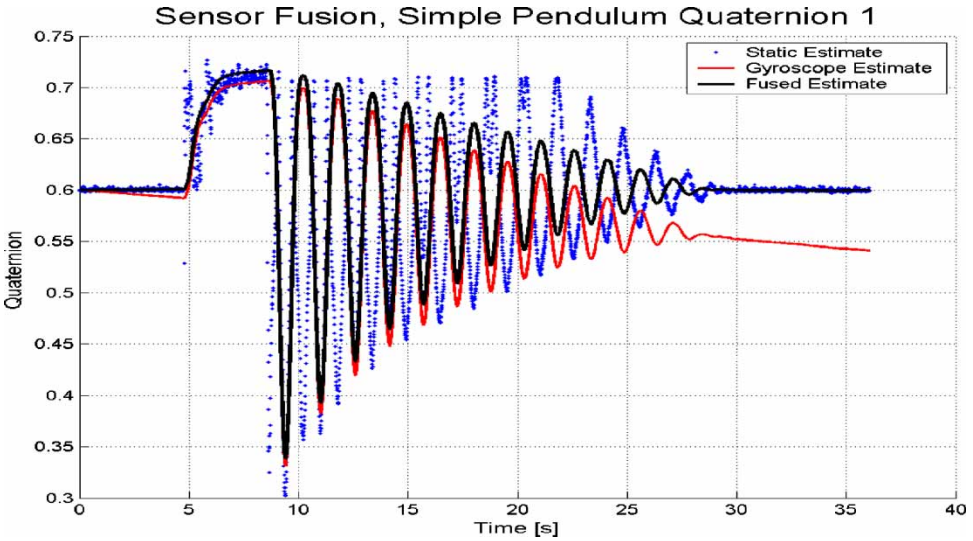

Figure 2. Pendulum swing in quaternion representation is presented. The pendulum is rotated slowly to the start position before being allowed to swing freely to rest. Although orientation requires four quaternions, (**Q**0, **Q**1, **Q**2 and **Q**3) only quaternion 1 (**Q**1) is shown for clarity. The static estimate, blue dots, the continuous estimate, red line, and the fused estimate, black line are shown.

local gravitational and magnetic field vectors described in (Figure 3).

$$\mathbf{R}_{\text{Global}} = \left[\mathbf{X}_{\text{Local}} \quad \mathbf{Y}_{\text{Local}} \quad \mathbf{Z}_{\text{Local}}\right]. \tag{1}$$

In the global coordinate system used by the IMU, the *Z*-axis points vertically upwards, the *X*-axis points to magnetic north and is normal to the *Z*-axis, and the *Y*-axis is normal to both *X* and *Z*-axes. In static situations $\mathbf{R}_{\text{Global}}$ is accurate, but in dynamic situations local acceleration of the sensor will affect the estimates of the Earth's gravitational field.

The continuous estimate

A second estimate of the rotation matrix is provided by integration of the angular velocity data provided by the gyroscopes. Quaternion representation of orientation is used to reduce computation. Quaternion representation may be readily converted to and from matrix representation or Euler's angles. Quaternions represent orientation by a single rotation (θ) about a unit vector (**U**). Quaternion representation of orientation has four components, one real and three imaginary, in vector form. The imaginary parts contain the *x*, *y* and *z* components of a unit vector (**U**) while the real part of the quaternion defines a rotation (θ) about **U** (Equation 2).

$$\mathbf{Q} = \left[\cos(\theta/2) \quad Ux{*}\sin(\theta/2) \quad Uy{*}\sin(\theta/2) \quad Uz{*}\sin(\theta/2)\right]. \tag{2}$$

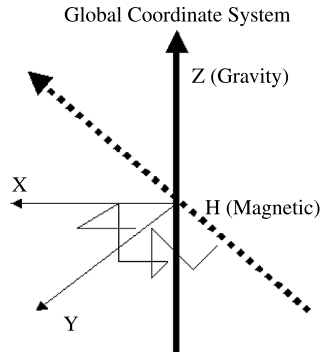

Figure 3. The global IMU coordinate system.

Care is required when forming quaternions because an ambiguity exists. A positive rotation about a positive unit vector is the same as a negative rotation about a negative unit vector.

The angular velocity quaternions are calculated from the gyroscope data (Equations (3)–(5)) and continuous orientation may then be calculated by quaternion multiplication of successive angular velocity quaternions (Equation 6). The initial orientation of the IMU in quaternion form ($\mathbf{Q}_{t=0}$) is required to begin the process; this is the constant of integration. It is derived from the mean of static estimates during the start period. It is important to note that quaternion multiplication in Equation (6) is different from matrix multiplication.

$$\Delta\theta = \frac{|\omega|}{\text{Sampling Rate}}, \tag{3}$$

$$\mathbf{U} = \frac{\omega}{|\omega|}, \tag{4}$$

where **U** is the unit vector.

The quaternion description of the change in orientation is presented in Equation (4) where U, x, y and z are the components of **U** from Equation (3).

$$\mathbf{\Delta Q} = \Big[\cos(\Delta\theta/2) \quad Ux*\sin(\Delta\theta/2) \quad Uy*\sin(\Delta\theta/2) \quad Uz*\sin(\Delta\theta/2)\Big]. \tag{5}$$

The orientation at time t is:

$$\mathbf{Q}_t = \mathbf{Q}_{t-1}*\mathbf{\Delta Q}. \tag{6}$$

The fusion process

The motion starts and finishes with stationary periods. The initial and final orientations of the pendulum as well as the initial and final bias of the gyroscopes are estimated during the stationary periods. The dynamic periods of motion are found by integrating the gyroscope channels between the static periods of motion.

This method assumes the period of action is relatively short (up to 30 s) and that it is bounded by stationary periods. If stationary periods are not present or the motion lasts longer than 30 s, fusion is still possible but a much more complex fusion algorithm is required. The method used for the pendulum swing is presented below:

(1) The static periods are identified from the gyroscope data using an angular velocity threshold.
(2) The gyroscope bias is calculated during each static period by taking the mean of each gyroscope channel over each static period.
(3) The gyroscope bias during the action period is then is then estimated by fitting a cubic spline between the initial and final gyroscope bias estimates.
(4) The calculated bias is added to the raw gyroscope measurements.
(5) The initial and final orientation of the action period are taken as the mean of the orientation during each static period. When taking the mean of an orientation in quaternion form, first decompose each quaternion into the angle (θ) and the unit vector (**U**), (see Equation (2)), then find the mean angle and mean unit vector before composing the mean quaternion. The algorithm also checks for ambiguity in the quaternions before composing the mean and ensures that the sign of the final quaternion is consistent with the initial quaternion.
(6) Two continuous estimates are then formed by integrating the corrected gyroscope data. The forward estimate is calculated by integrating from the start forward, using Equation (6), where the constant of integration ($\mathbf{Q}_{t=0}$) is the quaternion representation of the initial orientation. The backward estimate is calculated by integrating from the end back to the beginning.
(7) The forward and backward estimation of orientation are averaged over the period of dynamic motion using a cubic weighting function to obtain the fused estimate of orientation ($\mathbf{Q}_{\text{Fused}}$). Therefore, the early parts of the motion are weighted in favour of the forward estimate of orientation while the final parts of the motion are weighted in favour of the reverse estimate of orientation.
(8) An estimate of the 'true' gyroscope measurements ($\Delta\theta_{\text{Fused}}$) is made. In order to do this, Equation (6) is re-arranged to get the 'true' angular velocity quaternion ($\mathbf{\Delta Q}_{\text{Fused}}$) from the estimated 'true' orientation over time ($\mathbf{Q}_{\text{Fused}}$). Equation (5) is then re-arranged to get an estimate of the 'true' gyroscope measurements ($\Delta\theta_{\text{Fused}}$). This step is the quaternion equivalent to differentiation of position to get rate.
(9) The 'true' gyroscope measurements from step 8 are then subtracted from the raw gyroscope measurements to get an estimation of the dynamic bias over the action period. The dynamic bias is filtered using a bidirectional 3rd order Butterworth filter with a 0.5 Hz or lower cut-off frequency because the gyroscope specification gives the main component of the bias as low frequency drift.
(10) The low frequency dynamic bias is added to the raw gyroscope measurements.

Steps 6–10 should be iterated until the forward and backward integration of the gyroscope data give similar results. The true solution should be taken as the forward integration. If the data are good, convergence between the forward and backward estimates of orientation will be reached within two iterations. If more than two iterations are required the data are probably not suitable for this method of processing. The reasons for this may be: (1) The action periods are too long. (2) The global magnetic field is neither constant nor homogeneous. (3) The IMUs have a poor factory calibration. (4) There are periods of motion beyond the linear range of the sensors.

The video system

The motion of the pendulum was obtained using two Sony DRV-940E camcorders shuttered at 1/500 s. The digitising volume was calibrated using the static DLT procedure in the MaxTRAQ3D software (Innovision Systems Ltd.) that was used to manually digitise the motion of the pendulum. The MaxTRAQ software digitises individual fields giving a temporal resolution of 0.02 s (50 pictures per second) and the digitising image is displayed at a resolution of 720 × 576 pixels. The software is capable of sub-pixel accuracy in manual digitising mode.

Method

A wooden pendulum was constructed which rotated about a good quality cylindrical bearing. The pendulum was

90 cm long with a 50 cm transverse arm oriented along the axis of rotation. Two IMUs were attached to the pendulum 35 and 70 cm from the centre of rotation with the local IMU *x*-axis oriented along the pendulum shaft. The motion of the pendulum was recorded using two shuttered video cameras and the output of the IMUs was sampled at 100 Hz. Two different pendulum conditions were tested:

Normal motion in which the pendulum was set in motion by rotation about the *X*-axis and allowed to come to rest naturally; and
Stopped motion in which the pendulum rotation about the *X*-axis was stopped and started abruptly.

Three points on the pendulum, the centre of rotation, the end of the pendulum arm and the end of the transverse arm (shown by light red dots in Figure 3) were tracked in three dimensions using the MaxTRAQ software package. The projected angles of the pendulum motion were calculated from the three digitised points. Pendulum orientation was also determined from the output of the IMUs.

Of the nine possible projected angles only three were required to completely define the pendulum orientation. The three projected angles chosen were equivalent to rotations about the *X*-, *Y*- and *Z*-axes as defined in the camera global coordinate system (Figure 4). The projected angle about the *X*-axis contained the majority of the pendulum motion.

IMU accuracy was estimated by calculating the root mean square (RMS) difference between the three projected angles obtained from video motion analysis and the three projected angles obtained from the IMUs. The RMS difference between the projected angles of the two IMUs attached at different locations on the pendulum was calculated to estimate algorithm consistency.

The Data from the IMUs were processed in two different ways:

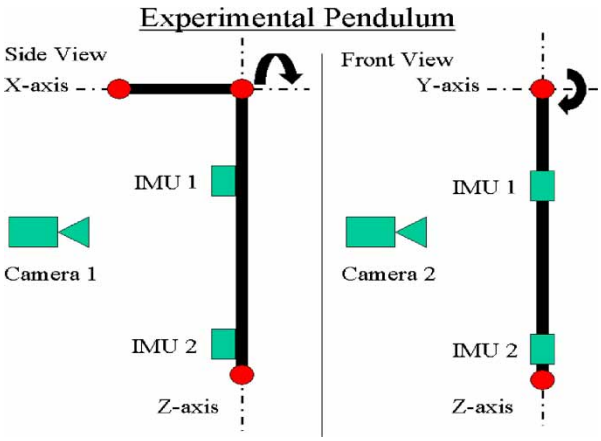

Figure 4. The experimental pendulum set up with camera positions and IMU placement.

(1) Using the manufacturer's Kalman filter with the recommended settings; and
(2) Using a custom fusion algorithm

Results

An example of the normal pendulum motion derived from video analysis is shown in Figure 5. The accuracy of pendulum position measurements using video analysis was estimated by considering the length of the transverse arm. The RMS length error was 4 mm which corresponds to an orientation error of $<0.5°$. As shown in Figure 5, the pendulum oscillates about the *X*-axis with very little motion about the *Y* or *Z*-axes. The same pendulum swing was measured by IMU using the Kalman Filter algorithm, Figure 6 and the custom fusion algorithm, Figure 7. Clearly, the output of the Kalman filter algorithm contains erroneous motion about the *Z*-axis

The RMS differences between the IMU estimates of pendulum orientation and the video analysis estimate of orientation are shown in Table 1. This illustrates the larger error in the Kalman filter estimate of orientation. Table 2 shows the difference in pendulum orientation obtained from IMU1 and IMU2 using both the fusion integration algorithm and the Kalman filter.

Discussion

The experimental pendulum swing was chosen because it was repeatable and a reasonable approximation of segment angular motion during gait. The cylindrical bearing substantially confined rotation to the *X*-axis. This was confirmed by the video analysis (Figure 5). However, there was a small amount of rotation about both the *Y*- and *Z*-axes, the mid green and light red lines in Figure 5.

The fusion algorithm performed very well. For test condition 1, the normal pendulum swing, the fusion algorithm output (Figure 7) is almost identical to the video output (Figure 5). The RMS error in orientation was between 0.8° and 1.3°, Table 1. The manufacturer supplied Kalman filter did not perform well; the RMS error was between 8.5° and 11.7° (Table 1). The peak orientation error for the Kalman filter solution was of the order of 30° about the *Z*-axis, which was found by comparing the light red line in Figures 5 and 6. The error is significantly larger than the RMS error of 3° specified by the manufacturer.

The fusion algorithm produced very similar results independent of the location of the IMU on the pendulum. The RMS difference was between 0.7° and 0.9° for the two locations on the pendulum (Table 2). The Kalman filter solution was less reliable for the two positions on the pendulum, producing significantly different estimations of orientation. The RMS error was between 3.3° and 4.0°.

The manufacturer's Kalman filter is a 'black box' so it is only possible to speculate why it performed poorly

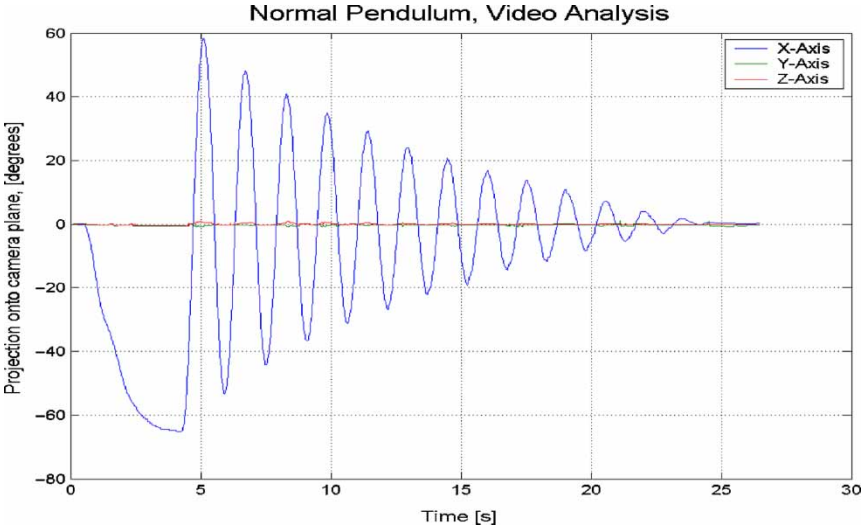

Figure 5. Video analysis of normal pendulum motion. Projected angles or rotations about the *X*, *Y* and *Z*-axes are represented by dark blue, mid green and light red lines.

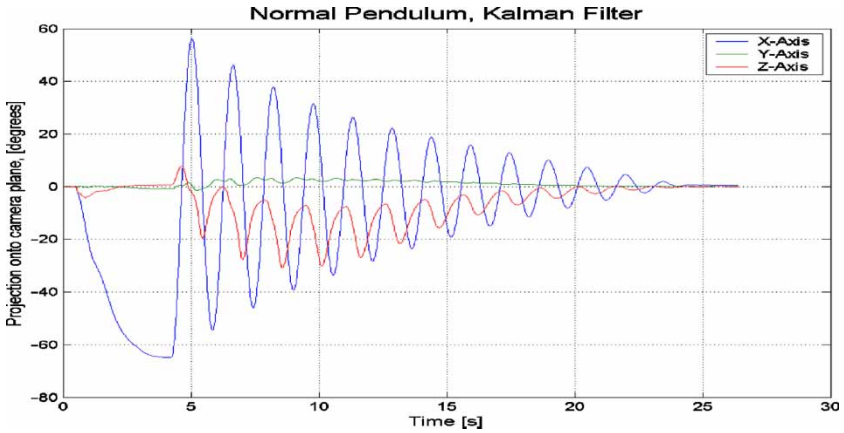

Figure 6. Kalman filter algorithm estimation of normal pendulum motion. Projected angles or rotations about the *X*, *Y* and *Z*-axes are represented by dark blue, mid green and light red lines.

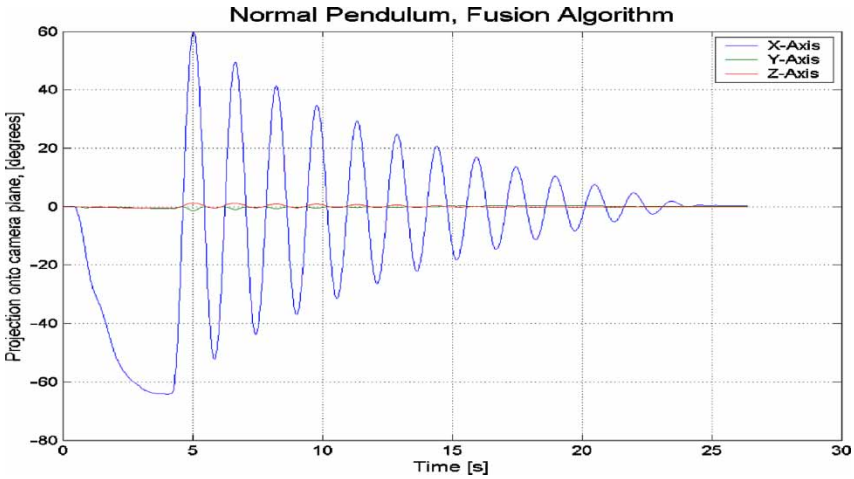

Figure 7. Fusion algorithm estimation of normal pendulum motion. Projected angles or rotations about the *X*, *Y* and *Z*-axes are represented by dark blue, mid green and light red lines.

Table 1. Accuracy: the RMS error of IMU estimates of orientation. Projected angles obtained from the video analysis are used as a reference.

Test condition	Fusion IMU 1 (°)	Fusion IMU 2 (°)	Kalman IMU 1 (°)	Kalman IMU 2 (°)
Normal pendulum	0.8	0.9	9.8	11.7
Stopped pendulum	0.9	1.3	8.5	8.6

in measuring a simple pendulum swing. The results show the Kalman filter supplied accumulates error as the length of the motion increases. For example, Figure 6 compared to Figure 5, shows the maximum erroneously reported *Z*-axis rotation occurs after about eight seconds of motion. This observation is in agreement with the recent findings of Luinge (2007) that orientation error increases with measurement duration.

The Kalman filter performed better in the second test condition, Table 1, where the pendulum was stopped and started abruptly (RMS error 8.6°). In the first test condition, the pendulum remained in motion for over twenty seconds and the centripetal and tangential acceleration experienced by the IMU were substantial, which probably increased the error in the Kalman filter solution (Figure 6). The solution improved as the magnitude of the pendulum swing decreased and the motion dependant accelerations reduced. In the case of the stopped pendulum trial the pendulum was stopped and restarted by the operator several times during the trial and so the periods of continuous motion were shorter. With shorter periods of motion the overall dynamic accuracy of the Kalman filter solution improved.

The authors speculate that the Kalman filter solution performed poorly for one of two reasons. The first possibility is that, during the periods of dynamic motion, the static estimate (Equation (1)) was used to correct for the expected low frequency drift of the gyroscopes. Unfortunately, the static estimate is not normally distributed about the true orientation in pendulum like motion. This is because the IMU rotates with the pendulum and the centripetal acceleration is always measured in the same local axis of the IMU. Therefore, the static estimate will be biased and, overtime, the static estimate will bias the solution. The second possibility is that the Kalman filter estimates the global acceleration as suggested by Luinge and Veltink (2005). However, the method used to estimate global acceleration requires that the orientation is known. Once the orientation error accumulates beyond a small threshold the global acceleration error may grow exponentially. If this is the case, it appears the error threshold for stability may depend on the magnitude of acceleration experienced by the IMU because the error decreased over the second half of the motion as the pendulum swing reduced (Figure 6).

Table 2. Reliability: the RMS difference between estimates of orientation obtained from two IMUs attached to the same pendulum at different locations.

Test condition	Fusion IMU 1 vs. IMU 2 (°)	Kalman IMU 1 vs. IMU 2 (°)
Normal pendulum	0.9	4.0
Stopped pendulum	0.7	3.3

In either case, the main problem for the Kalman filter used may be that the static estimate formed by Equation (1) is based on multiple cross-products as discussed by Brodie et al. (2007). Consequently, even if the inputs required to form the static orientation are normally distributed about the true values, the resulting orientation will probably be biased. The bias appears to be worse in parts of the world where the magnetic dip angle is greater and when high accelerations are present. The magnetic dip in our lab was about 60°.

The fusion algorithm presented here is good for short periods of motion (up to 30 s). It also requires stationary periods before and after the action. The algorithm will work best if the magnetic field measured by the IMUs in the start and finish positions is similar. In general this can be achieved in the laboratory for human motion by having the subject start and finish in the same calibrated position. The algorithm will work for all types of short motion provided the linear range of the sensors is not exceeded. The gyroscopes used in the IMUs have a linear range of 900° per second. The fusion algorithm presented has the advantage that a check on the quality of the raw data may be possible. If the solution converges with little iteration, then it is likely to be an accurate solution. Convergence is reached if the forward estimate of orientation is similar to the backward estimate of orientation.

The authors do not have a single fusion algorithm that is capable of accurate measurements in all situations and future research should concentrate on developing such an algorithm. The vendors of IMUs used should provide more specific details about the errors to be expected in different measurement situations, not just about the errors in a 'best case' scenario. If real time results are required a particle filter may be better than either a Kalman filter solution or a variation of the fusion algorithm presented here.

References

Brodie M, Walmsley A, Page W. 2005. Optimization of alpine ski race technique using sensor fusion. New Zealand Sports Medicine and Science Conference, Queenstown, New Zealand.

Brodie M, Walmsley A, Page W. 2007. The static accuracy and calibration of inertial measurement units (IMUs) for 3D orientation. Comput Methods Biomech Biomed Eng. Submitted.

Brodie M, Walmsley A, Page W. 2007. How to ski faster: art or science. 4th International Congress on Science and Skiing, St. Christoph am Arlberg, Austria.

Brodie M, Walmsley A, Page W. 2007. Fusion integration: COM trajectory from a force platform. J Appl Biomech. 23: 310–315.

Brodie M, Walmsley A, Page W. 2008. Fusion motion capture: A prototype system using IMUs and GPS for the biomechanical analysis of ski racing. J Sports Technol. (in press, doi: 10.1002/jst.6).

Giansanti D, Maccioni G, Benvenuti F, Macellari V. 2007. Inertial measurement units furnish accurate trunk trajectory reconstruction of the sit-to-stand manoeuvre in healthy subjects. Med Biol Eng Comput. 45:969–976.

Luinge HJ, Veltink PH. 2005. Measuring orientation of human body segments using miniature gyroscopes and accelerometers. Med Biol Eng Comput. 43:273–282.

Luinge HJ, Veltink PH, Baten CTM. 2007. Ambulatory measurement of arm orientation. J Biomech. 40(1):78–85.

Pfau T, Witte T, Wilson AM. 2005. A method for deriving displacement data during cyclical movement using as inertial sensor. J Exp Biol. 208:2503–2514.

Supej M. 2007. A step forward in 3D measurements in alpine skiing: a combination of an inertial suit and DGPS technology. 4th International Congress on Science and Skiing, St. Christoph am Arlberg, Austria.

Waegli A, Skaloud J, Ducret S, Roland P. 2007. Assessment of timing and performance based on trajectories from low-cost satellite positioning. 4th International Congress on Science and Skiing, St. Christoph am Arlberg, Austria (in press).

XSens Technologies B.V. 2004. Motion Tracker Technical Documentation Mtx-B. Version 1.03. www.xsens.com